Geomechanics and Engineering, *Vol. 5, No. 3 (2013) 195-221*
DOI: http://dx.doi.org/10.12989/gae.2013.5.3.195

Physical and numerical modeling of drag load development on a model end-bearing pile

R.F. Shen*, C.F. Leung[a] and Y.K. Chow[b]

Centre for Soft Ground Engineering, Department of Civil and Environmental Engineering, National University of Singapore, 1 Engineering Drive 2, Singapore, 117576

(Received March 17, 2012, Revised January 08, 2013, Accepted March 06, 2013)

Abstract. A centrifuge model study is carried out to investigate the behavior of pile subject to negative skin friction induced by pile installation, ground water drawdown and surcharge loading. A single end-bearing pile is examined as the induced negative skin friction would induce the most severe stress on the pile structural material as compared to friction piles. In addition, the behavior of the pile under simultaneous negative skin friction and dead/live loads is examined. To facilitate detailed interpretations of the test results, the model setup is extensively instrumented and involves elaborate test control schemes. To further examine the phenomenon of negative skin friction on an end-bearing pile, finite element analyses were conducted. The numerical analysis is first validated against the centrifuge test data and subsequently extended to examine the effects of pile slenderness ratio, surcharge intensity and pile-soil stiffness ratio on the degree of mobilization of negative skin friction induced on the pile. Finally experimental and numerical studies are conducted to examine the effect of applied transient live load on pile subject to negative skin friction.

Keywords: negative skin friction; dragload; pile; centrifuge model test; finite element method

1. Introduction

The induced shear stress along the pile-soil interface due to the relative downward settlement of surrounding soil with respect to pile shaft is commonly known as negative skin friction (NSF). It has been recognized that there exists three typical causes of NSF on piles; namely, soil re-consolidation after pile driving (see for example Fellenius 1972), lowering of the piezometric level (see for example Auvinet and Hanell 1981, Lee *et al*. 1998), and surcharge loading (see for example Johanesseen and Bjerrum 1965, Bozozuk 1981, Indraratna *et al*. 1992). Reported case histories revealed that in severe cases, the induced NSF could cause pile structural failure due to material overstress (see for example Kog 1987, 1990, Davisson 1993) or the pile settlement became excessive to beyond the serviceability limit of the super-structure (see for example Inoue 1977, Jacob and Kenneth 1997, Ng *et al*. 2008). Although many research studies had been conducted to investigate the phenomenon of NSF on piles, its mechanism is still not well understood and most of the design approaches are still largely empirical (Fellenius 2006).

*Corresponding author, Ph.D., E-mail: ceesrf@nus.edu.sg
[a]Professor
[b]Professor

http://www.techno-press.org/?journal=gae&subpage=7 ISSN: 2005-307X (Print), 2092-6219 (Online)

A pile with its tip resting on a hard stratum is commonly termed as end-bearing pile and would only settle very little even under a large load. Compared to friction pile, the magnitude of NSF or drag load induced on an end-bearing pile would be much more severe as the neutral point (NP) with identical pile and soil settlement is at or very close to the pile tip. The drag load is only of concern for the pile structural strength of end-bearing piles and is of no consequence for the pile geotechnical capacity. In view of the above, a centrifuge model study is conducted in the present study to investigate the load transfer characteristics of an end-bearing single pile subject to NSF. An elaborate testing scheme has been developed to induce NSF on a pile under different scenarios stated earlier. In addition, dead and live loads are applied at strategic test stages to investigate the pile behavior under simultaneous NSF and applied loads. This is followed by a detailed numerical study whereby the numerical model is first calibrated against the centrifuge test results. Further numerical studies are then carried out to investigate the degree of mobilization of NSF on end-bearing piles and the effects of dead and live loads on such piles subject to NSF.

2. Experimental setup and procedure

The phenomenon of NSF on pile is typically a time dependent process as the settlement of clay adjacent to the pile shaft could take years to complete. Centrifuge modeling technique is a useful tool to examine such problem as the soil consolidation process can be expedited up by N^2 times where N is the enhanced gravitational field on the soil model. As an example, a 10-hr model consolidation time in a centrifuge model at 80 g would be equivalent to 64,000 hrs or 7.3 yrs prototype soil consolidation time. All the centrifuge model tests in the present study were carried out at 80 g in the National University of Singapore Geotechnical Centrifuge. A schematic diagram of the model setup is shown in Fig. 1.

2.1 Soil container and model pile

The soil container was a stainless steel box featuring internal dimensions of 420 mm (length) × 420 mm (width) × 480 mm (height). Two sand hoppers were placed on top of the soil container. The holes at the base of the sand hoppers were blocked by a slider plate which could be pulled out by a horizontal hydraulic actuator to induce sand surcharge onto the model ground in-flight. Owing to Coriolis Effect, the sand would not fall vertically onto the soil surface (Taylor 1995) and guiding flaps shown in Fig. 1 were installed beneath the sand hoppers to direct the flow of sand to achieve a reasonably uniform surcharge on the model ground.

The model pile was fabricated from a hollow cylindrical aluminum tube with a Young's modulus of 7.1E + 4 MPa and yield strength of 220 MPa. A total of 9 levels of Wheatstone full-bridge circuits of semi-conductor strain gauges were installed along the pile shaft with SG1 placed near the pile tip and SG9 close to the pile head, see Fig. 1. The strain gauges were protected by a thin layer of epoxy resulting in a final outer diameter of 16 mm (1.28 m in prototypes scale) with an axial rigidity, EA, of about 2.38×10^3 kN (1.53×10^7 kN prototype). A vertical actuator was used to install the pile and apply loads in-flight at different test stages.

2.2 Model setup

A 62.5-mm thick rigid acrylic block was first placed at the center of the container. Dense silica

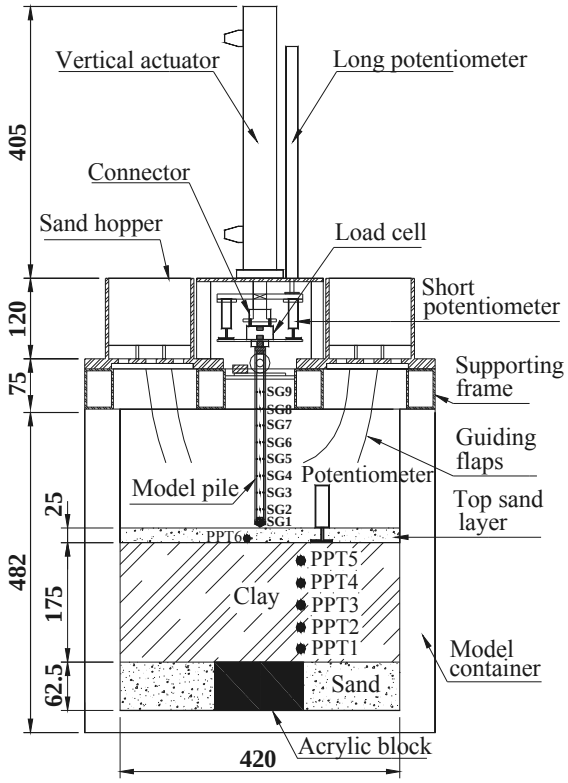

Fig. 1 Schematic model setup (unit in mm in model scale)

sand was then rained into the soil container to form a base layer of the same thickness around the acrylic block. De-aired water was subsequently introduced through a valve at the base of the container to saturate the sand. A slender aluminum frame carrying 5 pore pressure transducers (PPT) was then placed inside the container, see Fig. 1.

To prepare the clay, dry kaolin clay powder was remolded at a water content of 2 times its liquid limit in a soil mixer under vacuum for 3 hours. The clay slurry thus formed was poured into the soil container. The model container was subsequently mounted onto the centrifuge platform to subject the slurry to 80 g for 6 hrs to achieve over 95% consolidation, as verified by the PPT readings. The centrifuge was then spun down and a 25-mm thick loose sand layer was placed on top of the clay. This served as the top drainage layer to facilitate the simulation of water drawdown during a test stage.

With the model ground thus formed, two hoppers containing sand were mounted on top of the soil container. A potentiometer was installed on top of the clay surface at 150 mm from the container center to measure the soil settlement during the test. The model pile was connected to a load cell mounted to the piston of the vertical hydraulic actuator through a specially designed connector with a vertical slot. The piston of the vertical actuator would engage the lower flange of the slot when pushing the model pile downward during pile installation or when applying vertical load on the pile. When the piston was withdrawn half-way within the slot, it would disengage itself from the model pile. The completed model package was then spun up to 80 g again and the model

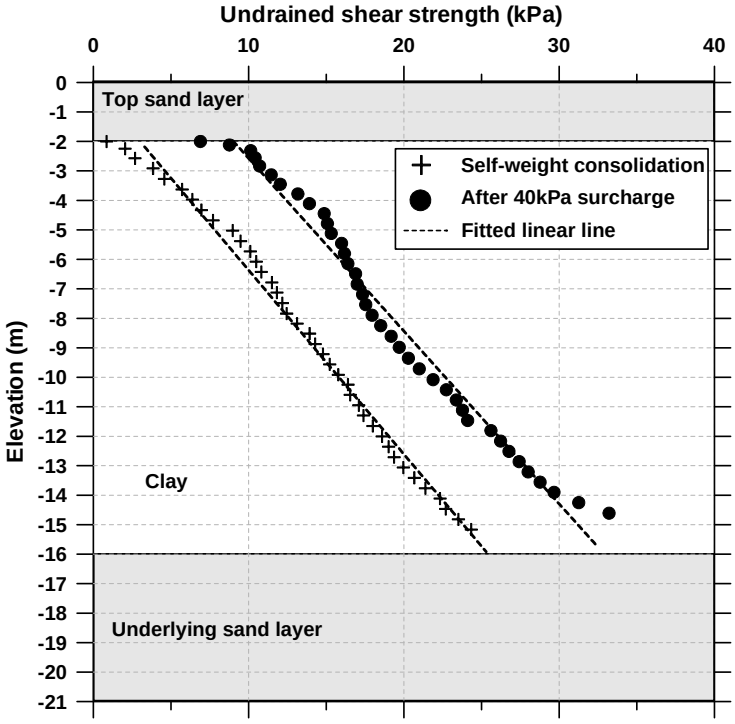

Fig. 2 Measured undrained shear strength of clay

clay ground would undergo further consolidation due to the self-weight of the clay and the top sand layer. The completed model ground featured a 25 mm thick (2 m prototype) sand layer overlying 175 mm (14 m prototype) normally consolidated soft clay underlain by rigid acrylic block/dense sand.

The undrained shear strength profiles of the soft clay after soil self-weight consolidation and after 40 kPa surcharge placement were measured using in-flight piezocone in a separate test. Fig. 2 reveals that the undrained shear strength of the clay increases reasonably linearly with depth for both cases. The placement of 40 kPa surcharge resulted in an undrained shear strength of about 10 kPa at the top of the soft clay layer.

2.3 Test procedure

The experimental procedure involved 6 test stages as follows:

(1) Upon completion of clay consolidation, the model pile was jacked into the model ground in-flight at a model penetration rate of 2 mm/s until the pile tip rested on the rigid acrylic block.
(2) After the vertical actuator was disengaged from the pile, the second test stage began involving the monitoring of pile load transfer characteristics based on strain gauge readings along the pile shaft. This stage also involved the dissipation of excess pore pressure generated from pile installation and the monitoring lasted for about 35 minutes (prototype consolidation time 156 days).
(3) The third test stage triggered the drawdown of water in the 25 mm (2 m prototype) thick top

sand layer and the corresponding monitoring of pile load transfer characteristics.
(4) The vertical actuator was then re-activated to apply compression load on the pile in Test Stage 4. The load transfer of the pile under simultaneous NSF and dead load was monitored.
(5) With the dead load still applied on the pile, the slider plate beneath the sand hoppers was activated to induce a 40 kPa sand surcharge onto the model ground. This Test Stage 5 monitored the pile load transfer characteristics under surcharge.
(6) After the excess pore pressure generated by the surcharge had fully dissipated, transient live loads were applied on the pile in 10 cycles. Test stage 6 incorporated this final monitoring of pile load transfer characteristics.

3. Centrifuge test results

Unless otherwise stated, all the test results are presented in prototype scale hereinafter.

3.1 In-flight pile installation (Test Stage 1)

Fig. 3 shows the development of excess pore pressure at various depths at a distance of 3 m from the pile center during pile installation. As expected, the deeper the PPT, the later it would

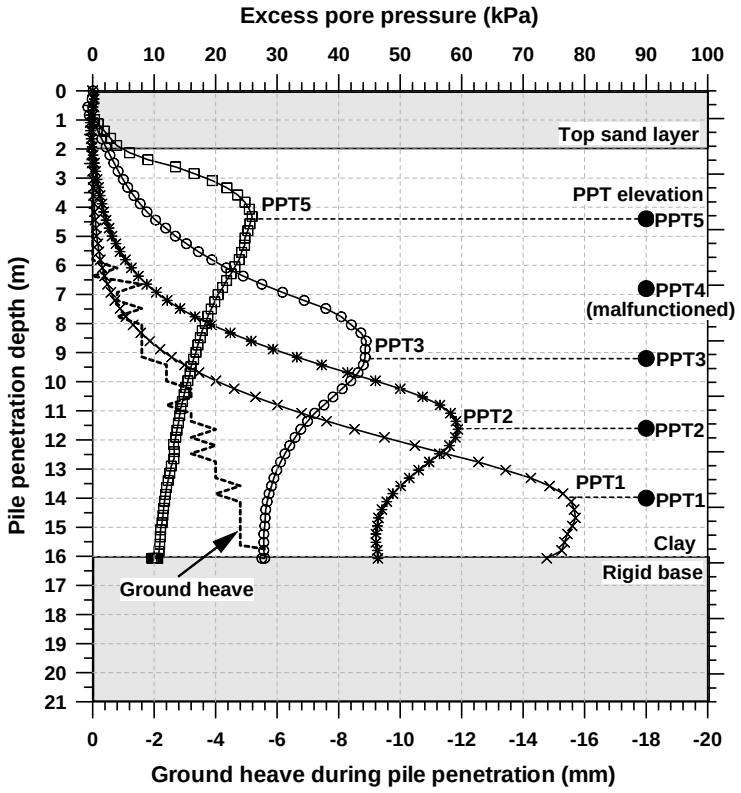

Fig. 3 Variation of excess pore pressure and ground heave as pile penetrated through model ground

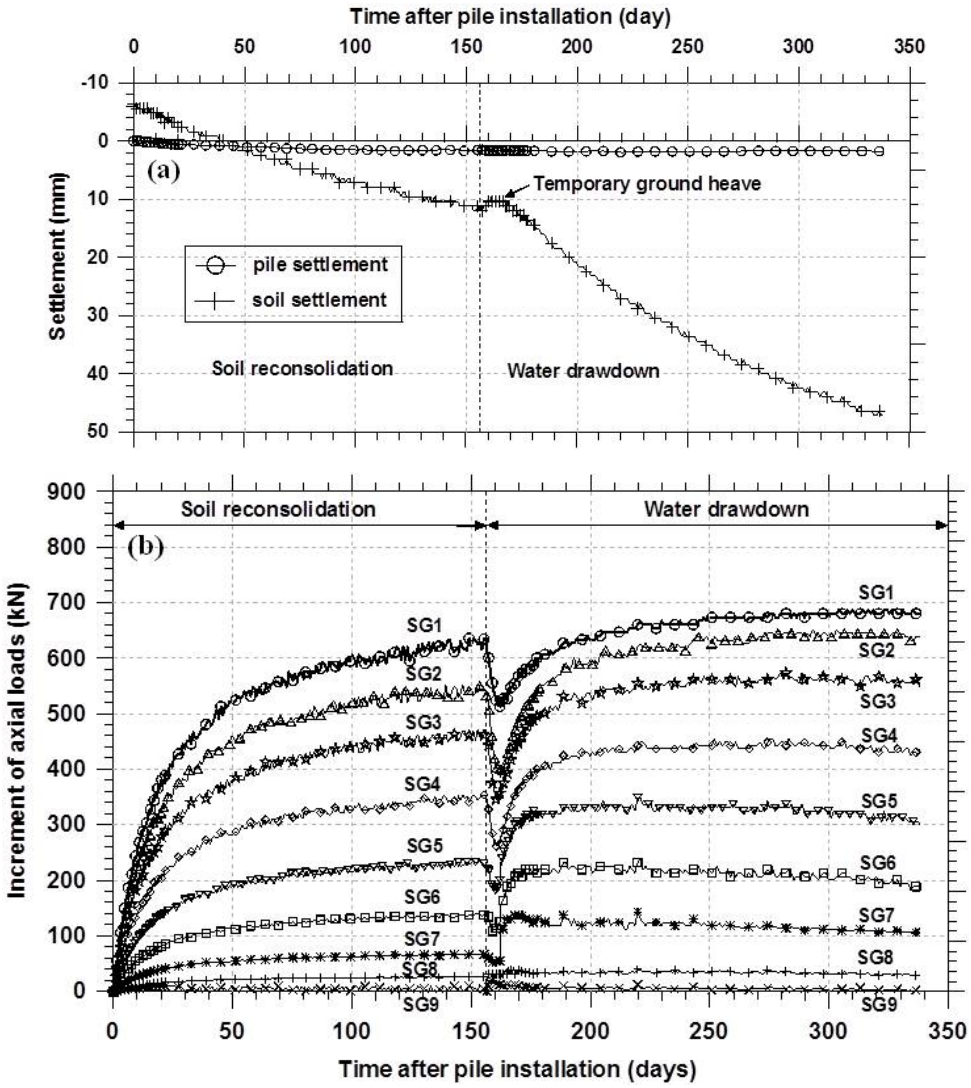

Fig. 4 (a) Settlement of soil and pile; and (b) mobilization of drag loads during soil re-consolidation and water drawdown stages

start to sense the penetrating pile. As an example, PPT5 located at 4.4 m depth began to experience excess pore pressure when the pile tip reached 1 m depth while PPT1 located at 14 m depth began to experience excess pore pressure when the pile tip reached 4 m depth. Fig. 3 reveals that each PPT registered the maximum excess pore pressure when the pile tip reached its respective elevation and the excess pore pressure then began to dissipate. These observations are similar to those observed by Leung *et al*. (1991) in a field test of driven piles in soft clay. Fig. 3 also reveals a maximum ground heave of about 6 mm.

3.2 NSF due to soil re-consolidation (Test Stage 2)

After pile installation, the excess pore pressure dissipated in both vertical and radial directions and soil re-consolidation was completed within 156 days. At 12 m from the pile center, the soil settled by about 18 mm due to soil re-consolidation in contrast to the initial heave of 6 mm during pile installation, resulting in a net soil settlement of about 12 mm, as shown in the left portion of Fig. 4(a). The settlement of the pile was noted to be negligible, confirming the rigid acyclic block functioned as a rigid base for the pile.

The development of NSF on piles due to re-consolidation of the remolded clay around the pile shaft has long been recognized. However, the only field data available to quantify such effect is reported by Fellenius (1972). Owing to ground settlement being much higher than that of pile, NSF is induced along the pile shaft, as shown in the left portion of Fig. 4(b). It is noted that the magnitude of NSF kept on increasing with a decreasing rate of increment as the soil reconsolidated. The maximum increment of axial load occurred at SG1 near the pile tip, and the increment reduced towards the pile head. The development of pile load transfer profile with time is plotted in Fig. 5. A maximum dragload of about 610 kN was induced near the pile tip at the end of soil re-consolidation being 156 days after pile installation. The neutral point (NP) persisted at the pile tip, in line with the findings reported by Johannessen and Bjerrum (1965) and Lee *et al*. (2002).

The total stress α (Tomlinson 1969) and the effective stress β (Burland 1973) methods are used to evaluate the dragload induced along the pile at the end of soil re-consolidation. The dragload P_N at any depth z can be calculated by

$$P_N = \int_0^z f_s^- dz \tag{1}$$

where the unit negative skin friction $f_s^- = \alpha C_u$ where Cu is the undrained shear strength of clay or $f_s^- = \beta \sigma_v$' where σ_v' is the vertical effective stress of soil. It should be noted that in fitting the α and β values to the test data, no attention was made to the 2 m top sand layer as the downdrag load contributed by the top sand layer was observed to be insignificant. The same phenomenon was also observed by Johannessen and Bjerrum (1965). For the α method, the undrained shear strength measured after self-weight soil consolidation (see Fig. 2) was used and the derived α value was 0.95, which is close to that reported by Leung *et al*. (2004) for the same clay.

The derived β value was 0.24, which is consistent with the β values reported for clays by Burland (1973), Garlanger (1974), Leung *et al*. (2004) and Gao *et al*. (2011). It is noted that around the neutral point near the pile tip, the NSF had not been fully mobilized due to small pile-soil relative settlement. As such, both α and β methods, which assume full mobilization of NSF from the ground surface to the neutral point, tend to over-predict the maximum dragload as illustrated in Fig. 5. The calculated maximum dragload of 705 kN is about 16% higher than the measured value of 610 Kn.

3.3 NSF due to water drawdown (Test Stage 3)

The increase in soil effective stress due to ground water drawdown is another major cause of NSF on piles. In an attempt to simulate such effect, the ground water level was drawn down by about 2 m from the ground level to the elevation of the top sand-clay interface at the end of the soil re-consolidation after pile installation. This was achieved by opening the drainage valve at the base elevation of the top sand layer while the centrifuge was in-flight. The reading of PPT-6 placed at the bottom of the top sand layer reveals that the water head was drawn down by about 1.5 m after 4 days and the full 2.1 m after 20 days, see Fig. 6. Owing to a smaller coefficient of permeability,

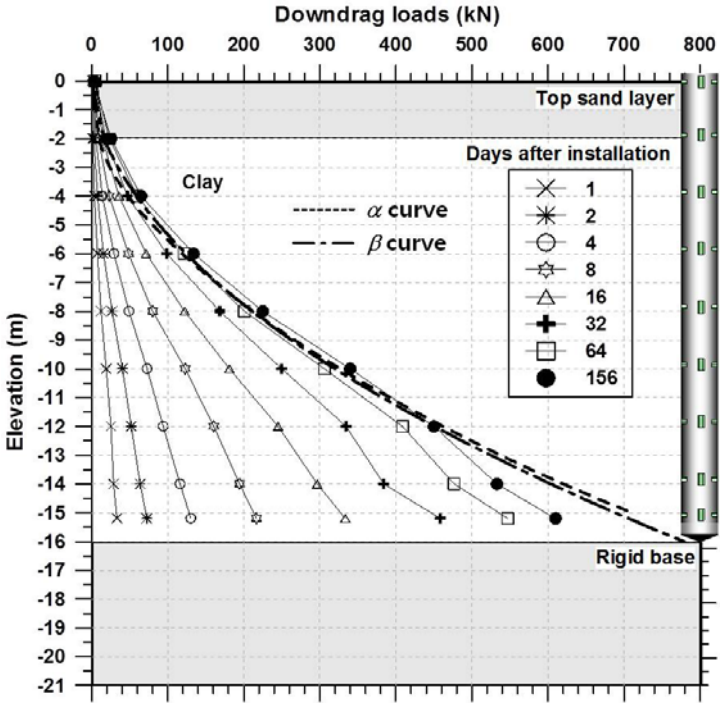

Fig. 5 Dragload profiles at some selected days during soil reconsolidation

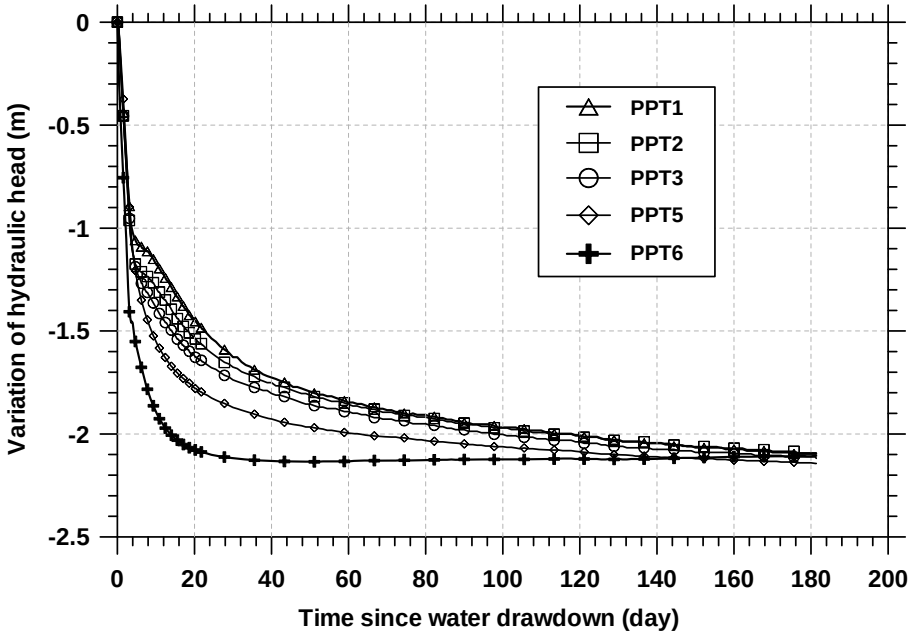

Fig. 6 Variation of hydraulic head on various PPTs since the start of water drawdown

Fig. 6 reveals that the reduction in hydraulic head in the clay generally lagged behind that of the sand layer. The clay only reached its final hydrostatic state in 180 days.

The variation of dragload during water drawdown is shown in the right portion of Fig. 4(b). Interestingly, the dragload was observed to reduce in the early stage of water drawdown and only started to increase after 4 days. This observation is consistent with the corresponding observed ground heave of about 2 mm shown in Fig. 4(a). Evidently, this temporary ground heave relieved the dragload on the pile.

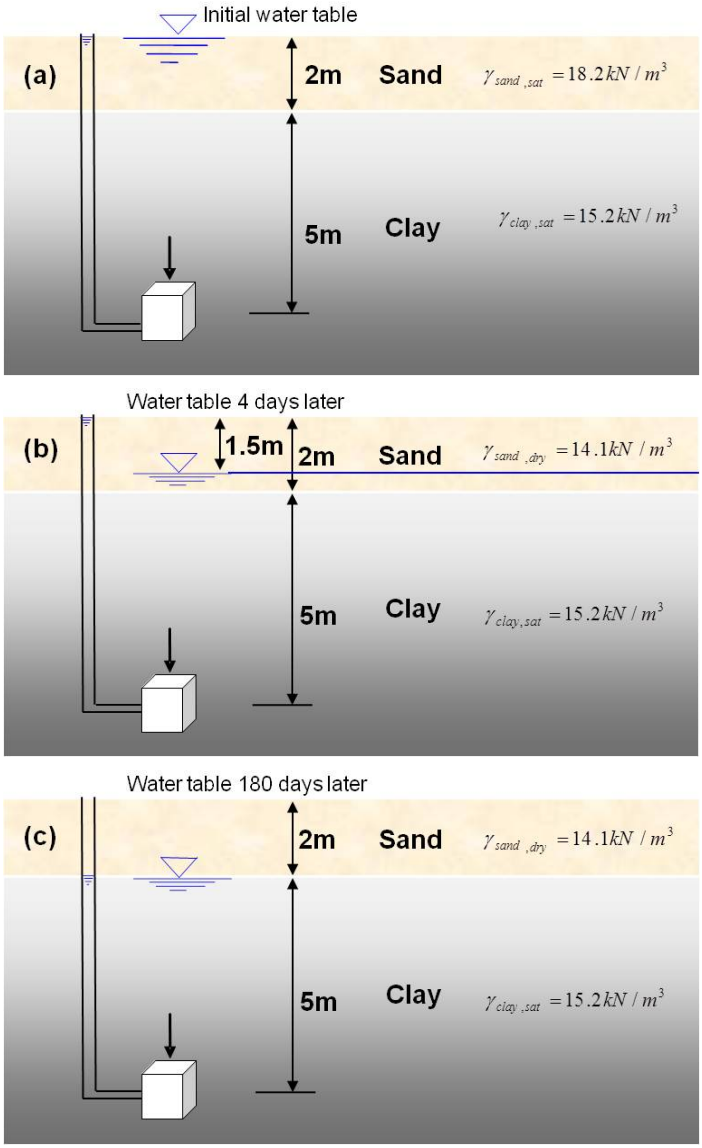

Fig. 7 Variation of ground water table and pore pressure at a soil element at (a) initial condition; (b) 4 days after water drawdown; and (c) 180 days after water drawdown

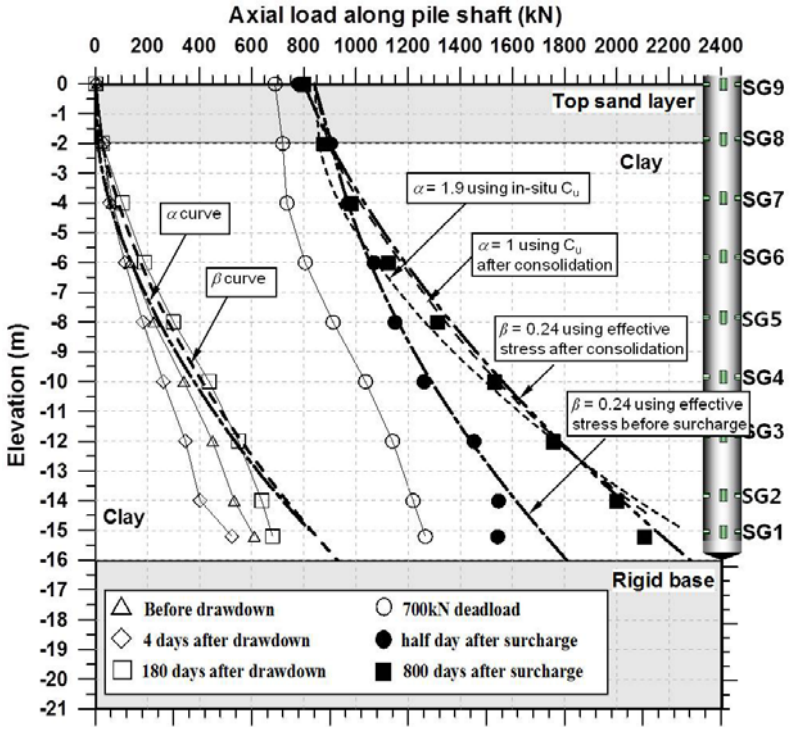

Fig. 8 Downdrag load profiles during water drawdown, application of dead load and surcharge test stages

Fig. 7 illustrates the variation of ground water table and the water head on a clay element at 7 m measured saturated unit weight, $\gamma_{sand,sat}$, and dry unit weight, $\gamma_{sand,dry}$, of the top sand layer is 18.2 below the ground surface before water drawdown as well as 4 and 180 days after drawdown. The kN/m^3 and 14.1 kN/m^3, respectively; while the saturated unit weight of the clay is 15.2 kN/m^3. The effective vertical stress before water drawdown is hence determined to be 42.4 kPa (Fig. 7a).

The water table was lowered by about 1.5 m 4 days after water drawdown but the clay was still at an undrained state due to its very low coefficient of permeability. As such, the effective vertical stress is 36.3 kPa that is a temporary reduction of 6 kPa (Fig. 7(b)). This causes the soil heave illustrated in Fig. 4(a) and temporary relief of NSF along the pile shown in Fig. 4(b). With the pore pressure completely dissipated in the long term as shown in Fig. 7(c), the effective vertical stress rose to 54.2 kPa which is about 11.8 kPa higher than that before the water drawdown. The gradual increase in vertical effective stress caused further soil consolidation settlement with time after the initial soil heave and induced NSF on the pile shaft as illustrated in Fig. 4(b).

The left 3 curves of Fig. 8 show the measured pile load distribution during this test stage. It is evident that the NSF first decreased after water drawdown and subsequently increased again before reaching the final state at 180 days after water drawdown. The α and β curves once again fit the test data of the final stage reasonably well except around the neutral point near the pile tip. This is expected as the relative soil-pile movement is considerably smaller around NP. The derived β value based on the increased vertical effective stress after water drawdown is 0.24, the same as that derived from the earlier soil re-consolidation stage. Using the undrained shear strength of clay

before water drawdown presented in Fig. 2, the derived α value is 1.1 and in excess of unity. It is believed that the α value should be about 1 as the soil strength should have increased marginally.

3.4 Application of deadload on pile (Test Stage 4)

Up to this moment, an accumulative maximum downdrag load of about 680 kN due to soil re-consolidation and water drawdown has developed near the pile tip as shown in Fig. 8. At this

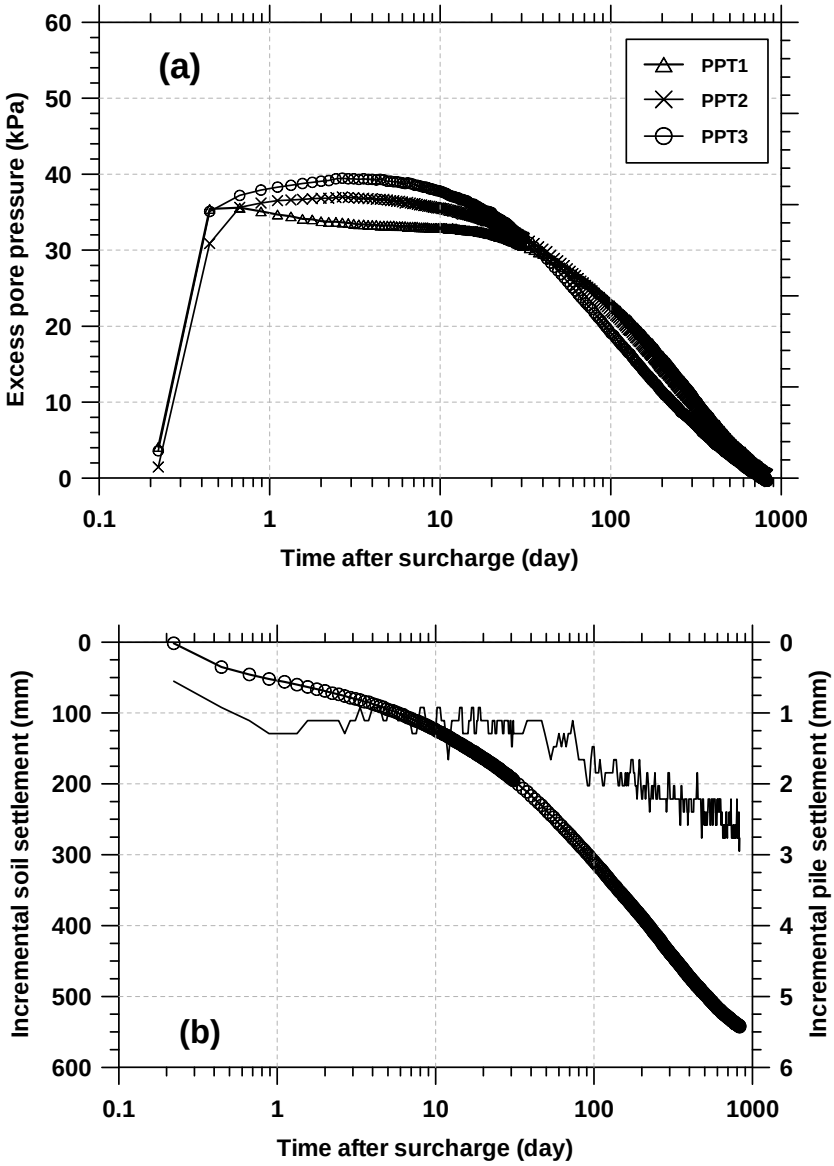

Fig. 9 Development of (a) excess pore pressure and (b) incremental soil and pile settlement upon surcharge loading

juncture, the vertical hydraulic actuator was re-activated to apply 700 kN load on the pile head. The load transfer along the pile shaft is represented by the middle curve with hollow circular symbol in Fig. 8. It can be seen that the applied load did not eliminate the NSF along the pile, but reduced the dragload to about 586 kN (maximum axial force at NP over the applied load at pile head), or about 84% of the applied load of 700 kN at the pile head. This observation is in line with that reported by Leung *et al*. (2004).

3.5 NSF due to surcharge (Test Stage 5)

Sand surcharge of about 40 kPa was subsequently placed on the soil in-flight. Fig. 9(a) show the development of excess pore pressure after surcharge application. As expected under undrained condition, the surcharge loading generated about 40 kPa excess pore pressure in the clay. The excess pore pressure then dissipated with time and essentially fully dissipated after 830 days. Fig. 9(b) shows that as the soil consolidated, the soil settlement increased with time and reached about 550 mm after 830 days. As an end-bearing pile, the corresponding maximum pile settlement of about 5.5 mm was only a small fraction of the soil settlement.

The application of dead load on the pile in the previous stage had caused the unit negative skin friction along the pile shaft to reduce by some extent to below the fully mobilized value. With the increase in soil settlement upon surcharge placement, Fig. 8 reveals that the loads along the pile shaft increased substantially along the whole length of pile shaft within a short time (refer to curve with solid circular symbols). By assuming that this load increment occurred in an undrained condition and the effective stresses in the clay remained the same as that prior to surcharge application, the derived β-curve fits the test data reasonably well using a β value of 0.24. It is noted that the load on the pile head at the original ground elevation also increased slightly to above the 700 kN dead load applied at Stage 4. This is attributed to the additional dragload induced along the surcharge-pile shaft interface.

The subsequent consolidation of the clay upon surcharge will increase the effective stress as well as shear strength of the clay. The β value using the increased effective stress at the end of the consolidation for fitting the long-term load distribution along the pile shaft is established to be 0.24, see Fig. 8. It can hence be deduced that the same β value can be used to determine NSF on pile as long as the correct effective stress along the pile has been employed. The back-analyzed α value is found to be 1.9 if original shear strength value is used while the value is about 1 if the increased soil strength at the end of consolidation (refer to Fig. 2) is used, see Fig. 8. As such, the common practice of using in-situ shear strength measured before the commencement of a project at the design stage would grossly under-estimate the dragload on a pile when the insitu soil is subjected to substantial surcharge resulting in substantial increase in shear strength of the clay after consolidation.

It should be noted that the much larger soil settlement under the surcharge loading caused the NSF to be almost fully mobilized even near the neutral point. As such, the calculated maximum dragload at the neutral point is much closer to the measured data, as illustrated in Fig. 8. In this case, the calculated value of 2197 kN only marginally over-estimated the measured value of 2098 kN by about 5%. This is in contrast to the previous stages when the soil settlement is substantially smaller and the mobilization near the NP is far from being fully mobilized, leading to a much larger discrepancy between the calculated maximum dragload and the measured value. As such, the magnitude of soil settlement is an important factor for the degree of mobilization around the neutral point. This aspect will be further explored later.

3.6 Effect of live loads on NSF (Test Stage 6)

Fellenius (1972) and Bozozuk (1981) observed in their respective field tests that the application of transient live loads on the pile head would reduce, eliminate and even reverse the NSF along the

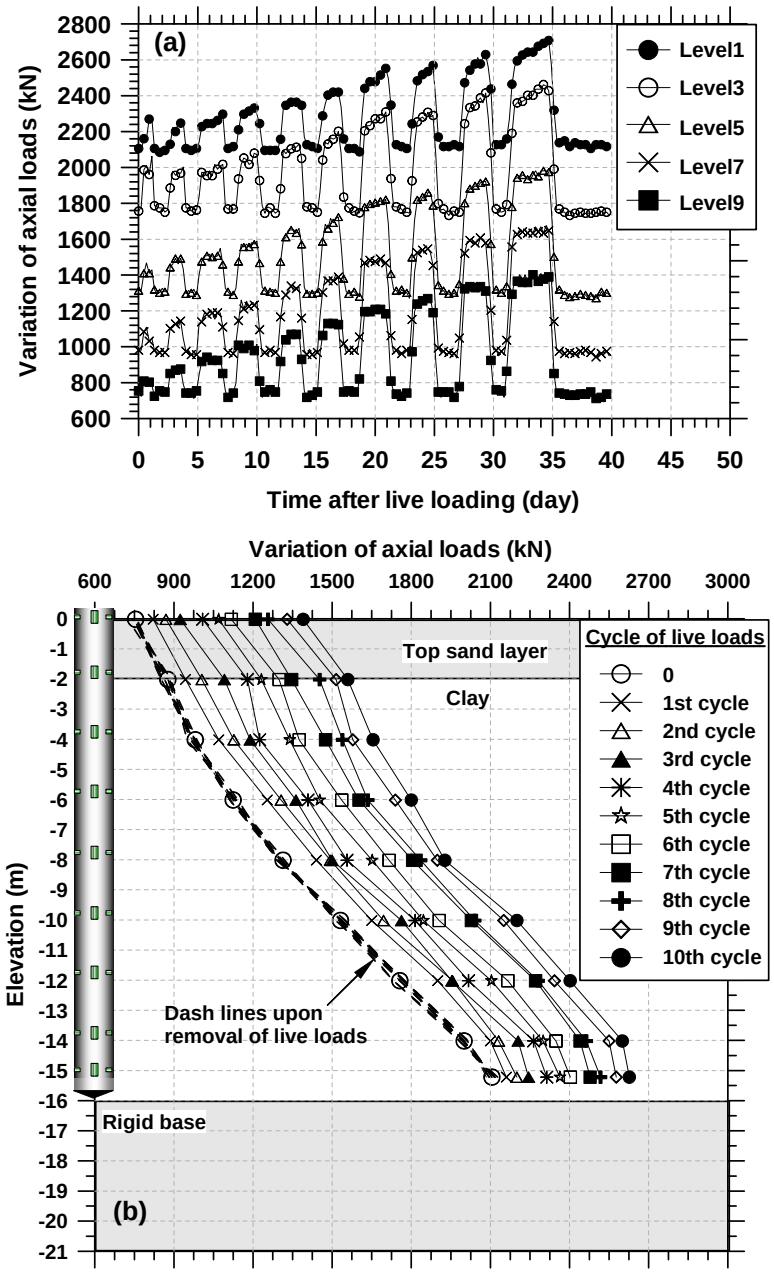

Fig. 10 Variation of axial loads during cylces of live loads (a) at selected gauge levels; and (b) along pile shaft

pile shaft. Bozozuk (1981) further postulated that transient live loads smaller than 2 times the maximum existing dragload would not contribute to the maximum dragload at NP of a pile. As such, either transient live loads or NSF, whichever is greater, needs to be considered in the design of pile subject to NSF. However, it should be noted that the above postulation is only supported by limited field studies and may not applicable for all cases. In the final test stage of the present study, live load was applied on the pile to study its effect on the existing NSF along the pile shaft. This was implemented by applying the load on the pile in cycles using a hydraulic actuator in a load control mode. A total of 10 load cycles of transient live loads was applied on the pile with the magnitude of live load increasing for each load cycle. The variation of load along the pile shaft (only selected gauges are shown to maintain clarify) during live loading is shown in Fig. 10(a). The magnitude of live load is reflected by the uppermost gauge SG9. It can be seen that the gauges along the pile shaft increased in tandem with the application of transient live loads at pile head and always reverted to the initial values upon removal of the live loads. Fig. 10(b) shows the axial pile load profiles for different live load cycles. The axial load profile at the end of surcharge as presented in Fig. 8 is re-plotted as the left-most curve of Fig. 10(b). Consistent with that observed in stage 4 during application of dead load, large proportion of the 10 cycles of live loads was observed to transfer to the NP at the pile tip contributing to the maximum load on the pile. Upon removal of the transient live loads, the load transfer curves reverted to that before the application of live loads without any residual effect as represented by the dashed curves cluttered closely together around the left-most curve of Fig. 10(b). The percentage of live loads transferred to the NP at various magnitudes of the transient live loads is fairly consistent ranging from 76% to 89% with an average value of about 83%.

The above observations further strengthen the idea that loads applied on a pile may be transferred to the NP under certain circumstances and the proposal that live loads up to 2 times the existing maximum dragload need not be considered in design may be an over-generalized statement. It should be noted that in the case history reported by Fellenius (1972), the slender concrete pile with a 300-mm diameter hexagonal cross section was driven through a deep deposit of 43 m top soft clay layer with a total pile length of 55 m. For the case of Bozozuk (1981), the 49-m long pipe pile with an outer diameter of 324 mm and a wall thickness of 6.35 mm was driven open ended through a 9-m height sand embankment into a deep deposit of highly compressible layered silty clay which extends to a depth of 73 m. However, in the present model test, the soft clay layer is only 14 m thick with a relatively rigid pile equivalent to a steel pipe pile with an outside diameter of 1.28 m and a wall thickness of 16 mm. It appears that the notion of "NSF and live loads need not be combined" is only applicable to long and slender piles installed through very deep deposit of soft soils. For stocky pile in relative shallow clay layer, the amount of load transfer to the NP contributing to the maximum load on the pile must be carefully quantified and evaluated in design. This issue will be further examined in the subsequent FEM analysis.

4. Numerical simulation of NSF on pile

In the present study, numerical analysis is also carried out to complement the centrifuge tests to delve deeper into the complex mechanism of NSF on piles. The numerical tool is first calibrated against the centrifuge model test data and further parametric studies are conducted to examine the issues on NSF mobilization factor and the effects of live load on NSF along the pile.

4.1 Back-analysis of centrifuge test data

Fig. 11 shows the axisymmetric configuration for the back-analysis of an end-bearing pile using geotechnical FEM software Plaxis-2D. The mesh is a geometric replication of the centrifuge model test setup shown in Fig. 1 and features 1880 15-node cubic strain triangular elements with 12 stress points each. Very fine elements are deployed adjacent to the pile while relatively coarse elements are used in far field areas. In the FEM mesh, the 2.5-m thick sand surcharge was simulated as solid elements instead of simplified uniformly distributed loads (UDL) such that induced dragload on the pile shaft within the sand surcharge can be captured as well. Some studies have shown that the incorporation of proper pile-soil interface elements is critical to capture the magnitude of NSF around the pile shaft correctly (see for example Lee *et al*. 2006, Lam *et al*. 2009). The left portion of Fig. 11 shows the interface elements available in Plaxis-2D program whose behavior is governed by the Coulomb criterion. The ultimate negative skin friction at the pile-soil interface, $f_{n,ult}$, is given by

$$f_{n,ult} = \sigma'_h \tan \varphi'_{\text{int}} + c'_{\text{int}} \tag{2}$$

where σ'_h is the normal effective stress on the interface element; c'_{int} and φ'_{int} are the effective cohesion and friction angle of the interface element, respectively. In most cases, the magnitude of c'_{int} is negligible. When negative skin friction at the pile-soil interface reaches the value given by Eq. (2), negative skin friction would be fully mobilized and permanent slip between the soil and

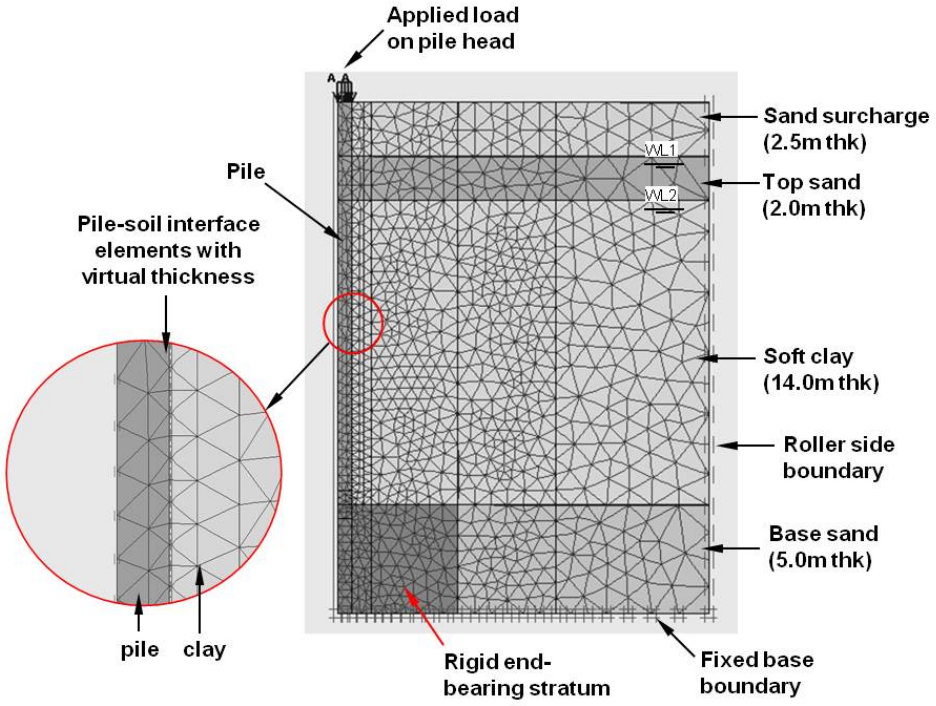

Fig. 11 FEM mesh for back-analyzing NSF on the end-bearing single pile

pile would occur.

Using the effective stress method, negative skin friction can be related to the effective vertical stress σ_v' by the coefficient β as

$$f_{n,ult} = \beta\sigma'_v \tag{3}$$

When using elastic-perfectly-plastic constitutive model such as Mohr Coulomb, the soil behavior is predominantly elastic under various loading stages including water drawdown and surcharge loading in the laterally confined model container analogous to that of a one-dimensional oedometer test condition. Under such circumstances, the ratio of effective horizontal and vertical stress is essentially governed by the soil effective Poisson ratio, ν', as

$$\frac{\sigma'_h}{\sigma'_v} = \frac{\nu'}{1-\nu'} \tag{4}$$

Combining Eqs. (2) to (4) and ignoring c'_{int}, the effective friction angle for the pile-soil interface element for the Mohr Coulomb model can be defined as

$$\phi'_{\text{int}} = \arctan\left[\frac{\beta(1-\nu')}{\nu'}\right] \tag{5}$$

For higher order of constitutive models like Modified Cam Clay model, the derivation of σ'_h/σ'_v can start with the following energy equation (Wood 1990)

$$qd\varepsilon_s^p + p'd\varepsilon_v^p = \sqrt{p'^2(d\varepsilon_v^p)^2 + M^2p'^2(d\varepsilon_s^p)^2} \tag{6}$$

where p' is the effective mean normal stress, q is the deviator stress, $d\varepsilon_s^p$ and $d\varepsilon_v^p$ are the incremental plastic deviator strain and plastic volumetric strain, respectively. Under the present laterally confined one-dimensional vertical compression condition

$$d\varepsilon_v = d\varepsilon_a + 2d\varepsilon_r \approx d\varepsilon_a \tag{7}$$

$$d\varepsilon_s = \frac{2}{3}(d\varepsilon_a + d\varepsilon_r) \approx \frac{2}{3}d\varepsilon_a \tag{8}$$

where $d\varepsilon_a$ and $d\varepsilon_r$ are incremental vertical and horizontal strains, respectively. On the other hand, the elastic volumetric strain component is typically negligible as compared to the plastic volumetric strain component during soil yielding and the Modified Cam Clay model disregards the elastic deviator shear strain. As such

$$\frac{d\varepsilon_v^p}{d\varepsilon_s^p} \approx \frac{d\varepsilon_v}{d\varepsilon_s} = \frac{3}{2} \tag{9}$$

Substituting Eq. (9) into Eq. (6) gives

$$\eta + \frac{3}{2} = \sqrt{\frac{9}{4} + M^2} \tag{10}$$

where η is the stress ratio defined by

$$\eta = \frac{q}{p'} = \frac{\sigma'_v - \sigma'_h}{\frac{1}{3}(\sigma'_v + 2\sigma'_h)} = \frac{3\left(1 - \frac{\sigma'_h}{\sigma'_v}\right)}{1 + 2\frac{\sigma'_h}{\sigma'_v}} \tag{11}$$

Combining Eqs. (10) and (11) leads to

$$\frac{3\left(1 - \frac{\sigma'_h}{\sigma'_v}\right)}{1 + 2\frac{\sigma'_h}{\sigma'_v}} + \frac{3}{2} = \sqrt{\frac{9}{4} + M^2} \tag{12}$$

or

$$\frac{\sigma'_h}{\sigma'_v} = \frac{9}{4\sqrt{M^2 + \frac{9}{4}}} - \frac{1}{2} \tag{13}$$

Combining Eqs. (2), (4) and (13), the effective friction angle of the interface element for the Modified Cam Clay Model can be defined as

$$\phi'_{\text{int}} = \arctan\left[\frac{4\beta\sqrt{M^2 + \frac{9}{4}}}{9 - 2\sqrt{M^2 + \frac{9}{4}}}\right] \tag{14}$$

Table 1 summarizes all the material parameters used in the numerical analyses which were obtained from standard laboratory tests. The FEM simulation procedure essentially follows the centrifuge test stages except for the pile jack-in process. As FEM simulation of pile jack-in process involves very large deformation and element distortion requiring intractable adaptive re-meshing techniques which is beyond the capacity of Plaxis-2D program, the pile was just "wished-in-place" in the present analysis. As such, the development of NSF due to soil re-consolidation after pile driving was not captured in the present FEM simulation. Coupled-consolidation analysis was conducted with the duration of each stage replicating that of the centrifuge model test.

Fig. 12 shows the comparison of numerical predictions of dragload along the pile shaft using both Modified Cam Clay (MCC) and Mohr Coulomb (MC) models against centrifuge test data at the end of water drawdown and surcharge stages. MCC model was used to simulate the soft clay and the friction angle of the soil-pile interface element is determined to be 17.3° using Eq. (14). It

Table 1 Parameters used for FEM back-analysis of NSF on piles

Material	Constitute model used	Bulk density γ_{bulk} (kN/m^3)	Cohesion C' (kPa)	Friction angle ϕ' (°)	Young's modulus E' (kPa)	Poisson ratio ν'	Permeability	Critical state parameters				Interface parameters	
								λ	κ	M	e_{int}	ϕ'_{int} (°)	c'_{int} (kPa)
Top sand layer	Mohr Coulomb (MC model)	18.2	0.1	30.0	8,000	0.30	1.0E-0.4	-	-	-	-	29.2	0.1
Soft clay	Modified Cam Clay (MCC model)	15.5	-	-	-	-	2E-08	0.25	0.05	0.94	1.72	17.3	0.1
	Mohr Coulomb (MC model)	15.5	0.1	24.0	Before surcharge $E'top = 970$ $\Delta E' = 166$ / After surcharge $E'top = 1300$ $\Delta E' = 180$	0.35	2E-08	-	-	-	-	24.0	0.1
Base sand layer	Mohr Coulomb (MC model)	19.2	0.1	38.0	55,000	0.30	1.0E-05	/	/	/		29.2	0.1
Surcharge dry sand	Mohr Coulomb (MC model)	16.0	0.1	35.0	10,000	0.30	1.0E-04	-	-	-	-	29.2	0.1
Pile	Linear elastic	9.5*	-	-	1.2E+07	0.20	-	-	-	-	-	-	-
End-bearing Perspex	Linear elastic	24.0	-	-	3.1E+06	0.20	-	-	-	-	-	-	-

*Taking into account the hollow the model pile

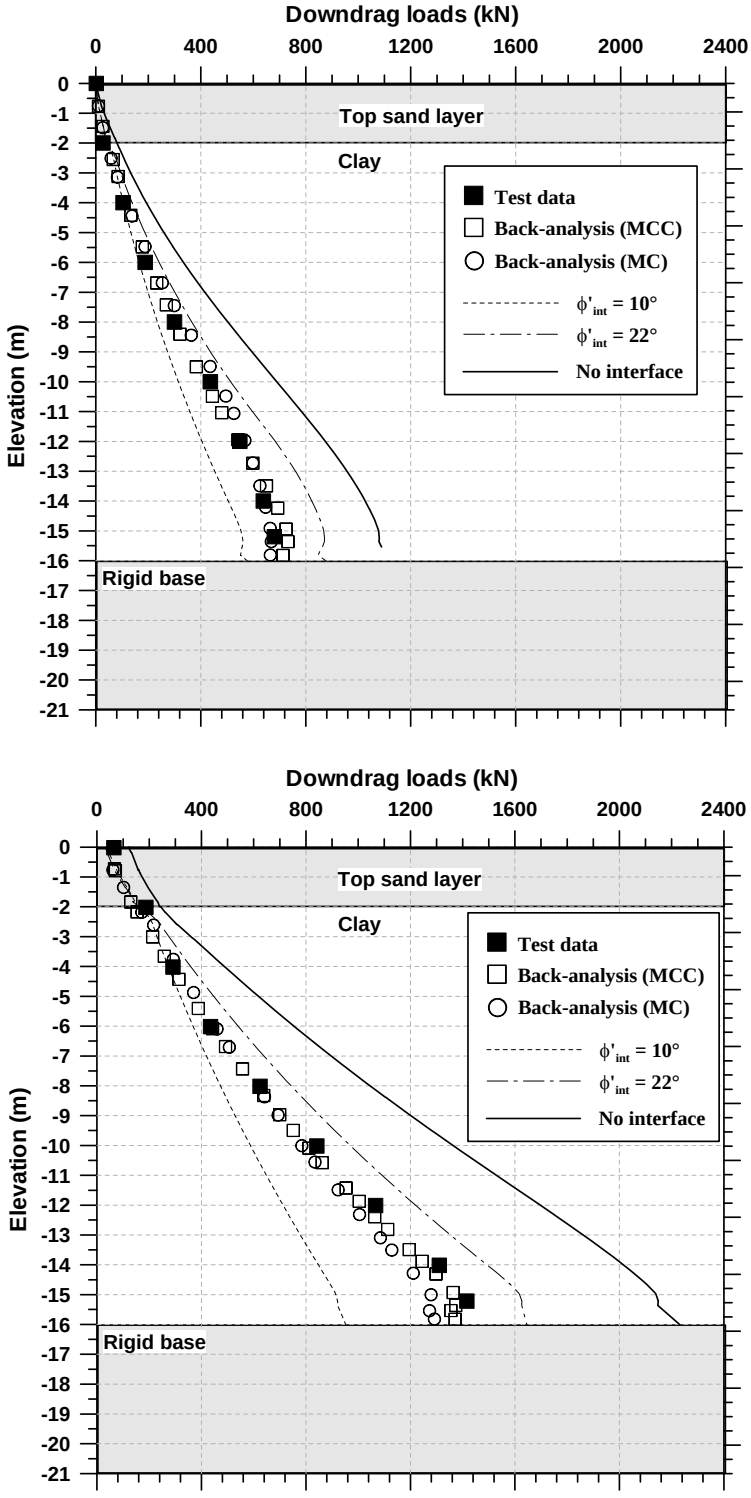

Fig. 12 FEM analysis of dragload at the end of (a) water drawdown; and (b) surcharge stages

is evident that the numerical results not only capture the neutral point of the end-bearing pile at the pile toe, but also match the magnitude of the dragload closely. The calculated maximum dragload along the pile is 732 kN and 1375 kN at the end of water drawdown and surcharge stages, respectively. These values are within 8% of the corresponding measured dragloads of 680 kN and 1416 Kn.

The simpler MC model is often used in engineering practice. The corresponding interface friction angle is determined to be 24° using Eq. (5). It can be seen from Fig. 12 that the calculated dragloads using MC model agree with those using MCC model and the measured data. As such, the simpler MC model is also competent to capture the correct NSF if the correct interface friction angle is employed.

To further demonstrate the effect of pile-soil interface friction angle, parametric studies were carried out using nil interface and interface friction angle of 10° and 22°. Fig. 12 shows that the numerical prediction of NSF essentially increases or decreases in tandem with the value of interface friction angle. All the above 3 cases deviate greatly from the measured data. The above analyses clearly demonstrate that in FEM analysis of NSF problem, interface elements must be applied at the pile-soil interface and assigned with the correct interface friction angle.

4.2 Degree of mobilization

The centrifuge model test data have consistently demonstrated the partial mobilization of NSF around the neutral point under various scenarios. As such, both α and β methods would overestimate the downdrag load on a pile. Poulos and Davis (1980) proposed a "correction factor" for cases where full slip does not occur around the neutral point. Matyas and Santamarina (1994) reported that the relative stiffness between the soil and the pile would substantially alter the partially mobilized zone. So far, no conclusive guidelines in this aspect are available although such concept has been mentioned in some Codes of Practice for foundations, see for example Singapore CP4 (2003). A better understanding and evaluation of the mobilization factor will directly lead to a better estimation of maximum dragload on a pile which is important in the design of piles with NSF.

To gain a better understanding on the mobilization factor under various pile and soil conditions, further numeric parametric studies were conducted. Since the simpler MC model is capable of replicating the NSF of the pile as illustrated earlier, it was adopted for this numerical parametric study. In this regard, the following symbols are defined:

(1) η – degree of mobilization of NSF

$$\eta = \frac{Q_{n,mob}}{Q_{n,\beta}} \tag{15}$$

where $Q_{n,mob}$ is the mobilized dragload and $Q_{n,\beta}$ is the calculated maximum dragload using the conventional β method and given as

$$Q_{n,\beta} = \int_0^{Zn} \beta \sigma'_v dz \tag{16}$$

in which Z_n is the depth of the neutral point and β assumes a typical value of 0.24 for clay based on the present model test data.

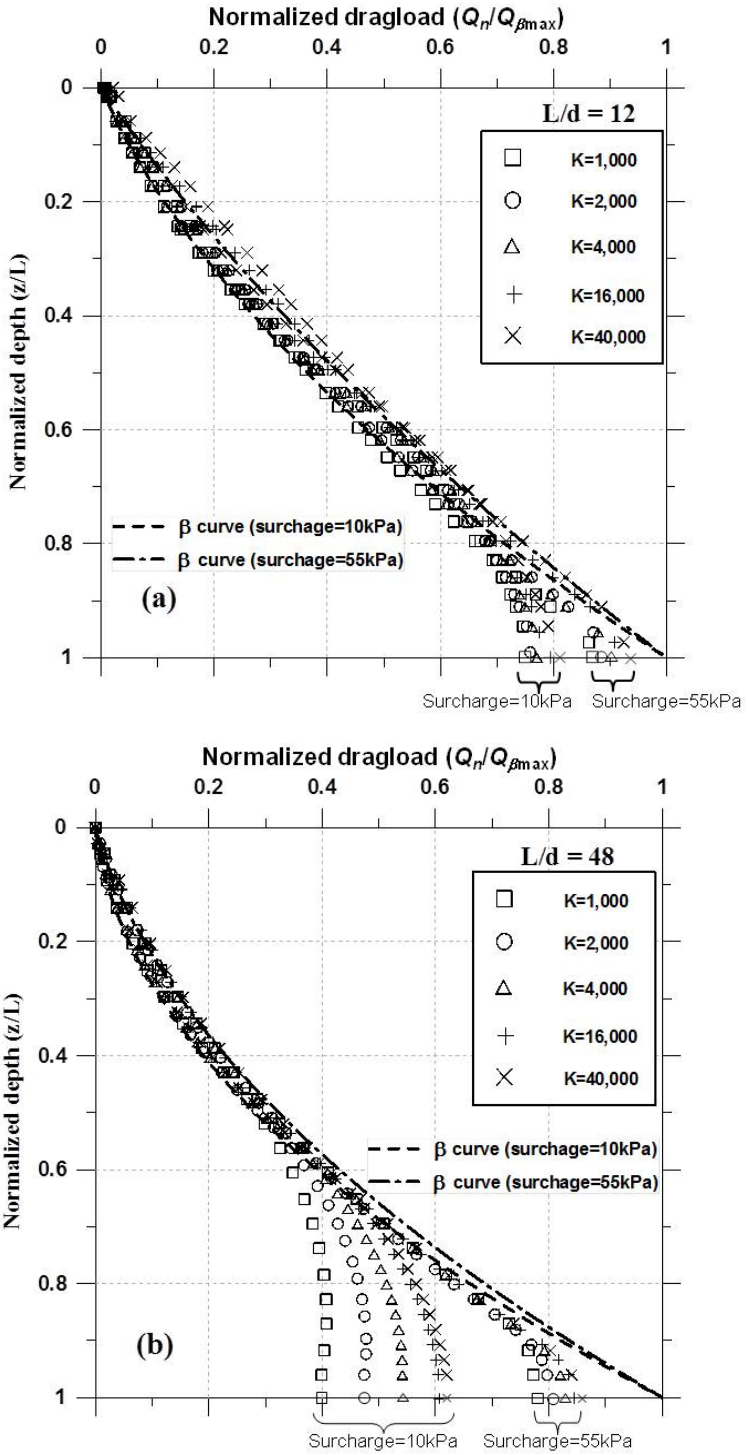

Fig. 13 Normalized dragload for (a) stocky pile; and (b) slender pile under various K values and surcharges

(2) K – pile-soil stiffness ratio (Poulos and Davis 1980)

$$K = \frac{E_p R_A}{E_s} \tag{17}$$

where E_p and E_s are the Young's modulus of the pile and soil, respectively. R_A is the pile section ratio defined as

$$R_A = \frac{A_p}{\pi d^2 / 4} \tag{18}$$

where d is the pile outer diameter and A_p is the solid area of the pile cross section. For the solid pile adopted in the present study, $R_A = 1$.

(3) L/d – pile slenderness ratio, where L and d are the pile length and diameter, respectively.

Two pile slender ratios of 12 and 48 were analyzed for the 1-m diameter end-bearing pile. For each slender ratio, the pile-soil stiffness ratio, K, was varied from 1,000 to 40,000, while the surcharge was gradually increased from 10 kPa to 70 kPa. For clarity of presentation, only the analysis results of surcharge 10 kPa and 55 kPa are presented in Fig. 13. It should be noted that the depth z has been normalized by the clay depth L, while the dragload along the pile shaft has been normalized by the maximum dragload at the neutral point, $Q_{n,\beta}$. For comparison purpose, the normalized β curves are also plotted in Fig. 13. In all the cases, the normalized dragload around the neutral point (the pile tip in the present case) is less than the corresponding β curves which assume fully mobilization of NSF at neutral point. For a stocky pile with L/d of 10 shown in Fig. 13(a), the normalized dragload on the pile is not much affected by the pile-soil stiffness ratio K, regardless of magnitude of surcharge intensity. This is understandable as an end-bearing stocky pile would experience small pile settlement under load and the relatively large soil settlement becomes dominant and causes a larger degree of mobilization of NSF. On the other hand, for a slender pile with L/d of 48 shown in Fig. 13(b) with a relatively small magnitude of surcharge loading of 10 kPa, the relative pile-soil settlement tends to increase as pile-soil stiffness ratio K increases, resulting in a substantial increase in the degree of mobilization of NSF. With a much larger surcharge magnitude of 55 kPa, the significantly larger soil settlement results in a greater relative pile-soil settlement. This leads to a much larger degree of mobilization of NSF with the effect of K diminishing as shown in Fig. 13(b).

The results of all the analyses for various pile slenderness ratio L/d, pile-soil stiffness ratio K and intensity of surcharge loading q are summarized in Fig. 14. The following generalized behavior can be deduced:

(a) For the same L/d, the degree of mobilization of NSF increases with surcharge intensity but tends to taper off after surcharge intensity q beyond 40 kPa revealing full pile slip beyond this surcharge magnitude. On the other hand, an increase in K tends to increase the degree of mobilization and its influence is far more substantial for a slender pile (see Fig. 14(d)).

(b) For the same K, the degree of mobilization of NSF tends to increase with q but decrease with increasing L/d.

(c) For the same q, the degree of mobilization of NSF generally increases with K. This is more evident for slender piles than for stocky piles. A very large q and hence very large soil settlement would greatly increase the degree of mobilization around the neutral point.

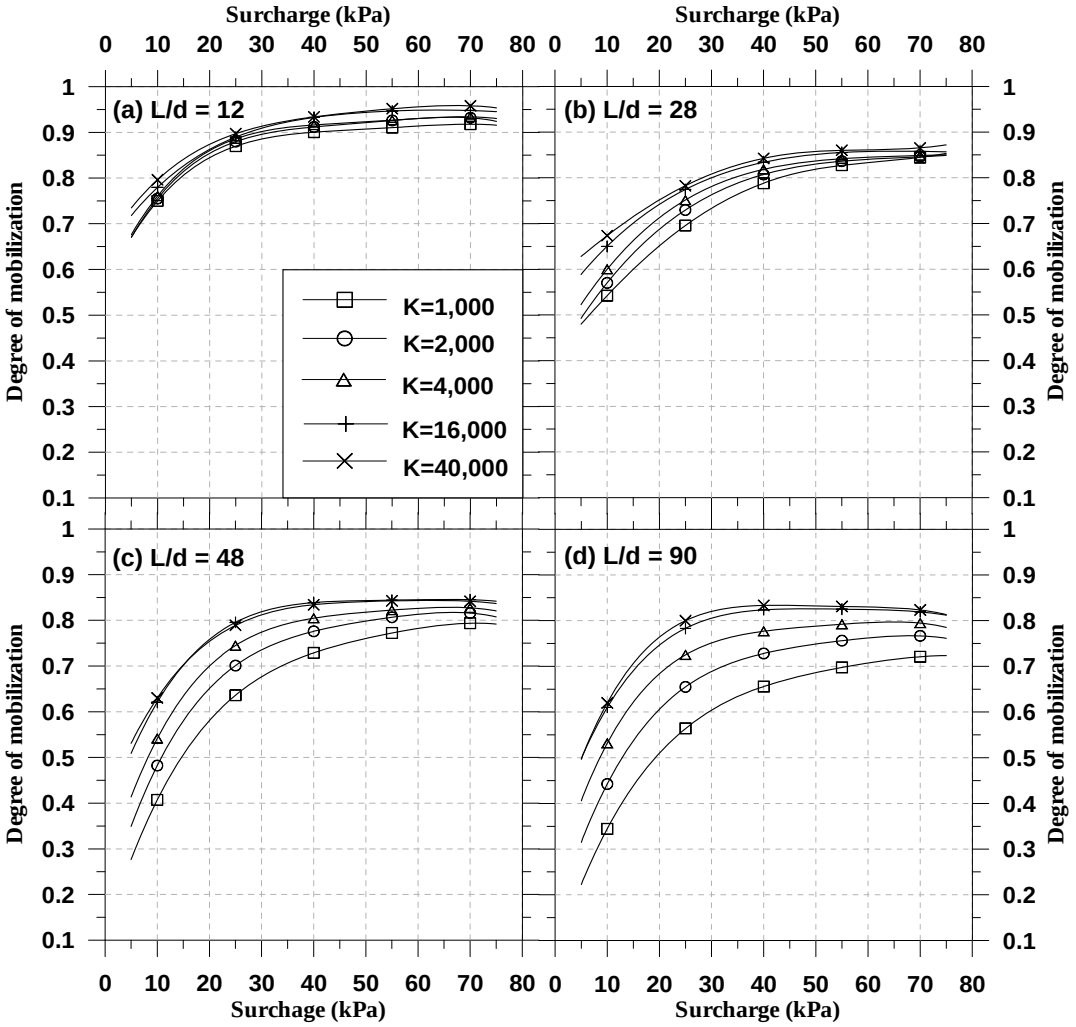

Fig. 14 Variation of NSF degree of mobilization with pile slenderness ratio, pile-soil stiffness ratio and surcharge intensity

It can be seen from Fig. 14 that the degree of mobilization of NSF can vary widely ranging from 35% to 95% depending on the pile-soil conditions and surcharge intensity. This parametric study illustrates that numerical study is able to simulate the degree of mobilization of NSF well as long as the correct pile-soil interface is adopted in the analysis. For the case of simple MC model, the degree of mobilization of NSF is taken care of by the elastic stress-strain soil response before soil failure upon which full pile slip occurs at the given pile elevation.

4.3 Effect of transient live loads on NSF

As mentioned previously, a limited number of field tests on NSF revealed that negligible percentage of transient live loads was transferred to the neutral point (Fellenius 1972, Bozozuk

1981). Such field observations have prompted a postulation that transient live load needs not be considered when evaluating the maximum load at NP on a pile. However, the present centrifuge model tests reveal that a fairly large percentage of the applied load has been transferred to the NP contributing to the maximum load in the pile under the present test configuration. Further parametric FEM analysis was hence conducted with the same range of K, L/d, and q as in the previous section. The simple MC model was again adopted here. After the development of NSF upon application of surcharge, loads were applied at the pile head in steps with the final magnitude up to 2 times the existing maximum dragload due to the surcharge. For clarity, only selected analysis results for surcharge of 10 kPa, 40 kPa and 70 kPa, and K of 1000, 4000 and 16000 are presented in Fig. 15. The results show that the percentage of applied live loads transferred to NP is not significantly affected by the magnitude of surcharge q, and independent of the magnitude of applied dead load on the pile. On the other hand, the percentage of applied load transferred to the NP tends to increase in tandem with pile-soil stiffness, K. The stocky pile with L/d of 12 generally has a much higher percentage of load transferred to the NP than the slender pile with L/d of 48.

Fig. 16 summarizes the variation of percentage of applied live loads transferred to the NP under various K and L/d. The results reveal that the percentage of applied live loads transferred to the NP increases with increasing K with no further increase when K exceeds 15,000, but decreases with increasing L/d. It can be seen that only with very large L/d of over 90, and very low K of less than 1000, can the percentage of transient live loads transferred to the neutral point be reasonably neglected.

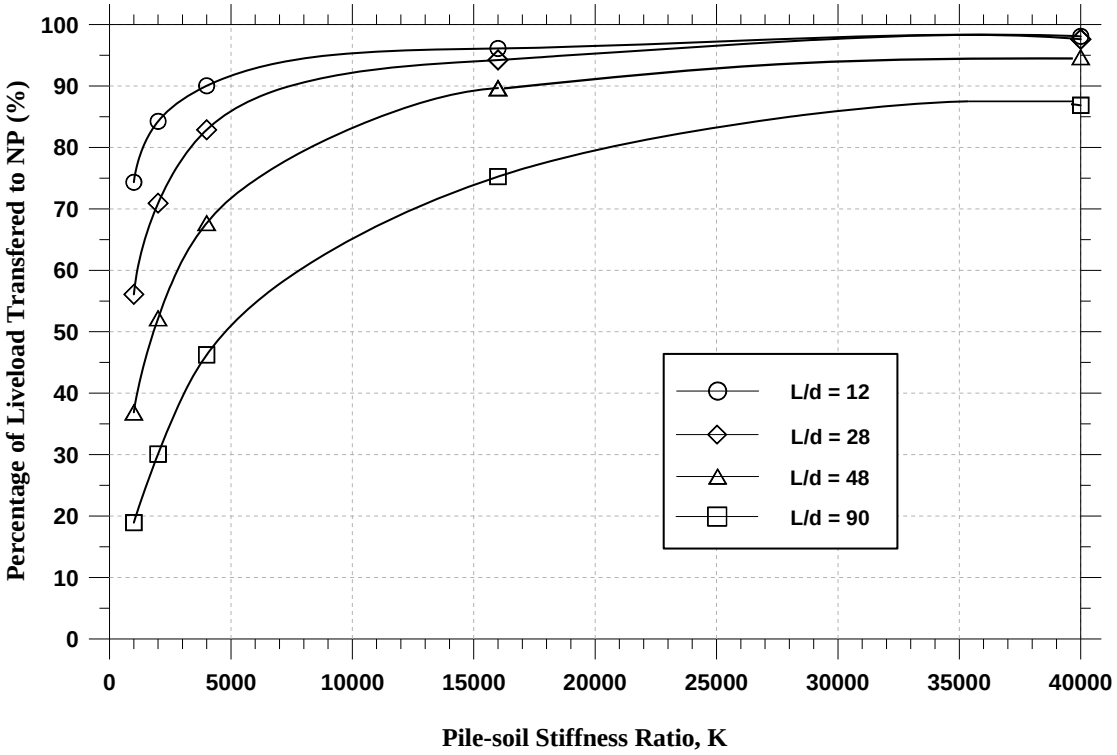

Fig. 16 Percentage of transient live loads transferred to neutral point at various pile-soil conditions

Figs. 14 and 16 may be used as a practical guide to estimate the degree of mobilization of NSF and the percentage of transient live load transferred to the neutral point for an end-bearing pile under various pile-soil conditions.

5. Conclusions

Centrifuge model study has been carried out to investigate the behavior of an end-bearing pile subject to negative skin friction (NSF) induced by the soil re-consolidation after pile installation, water drawdown and surcharge. In additional, the behavior of pile subject to simultaneous NSF and dead/live loads was also studied. Based on the present test configuration, the following findings are established.

(a) Owing to dissipation of pore pressure generated in the soil due to pile installation, NSF was observed on the pile and the neutral point was confirmed to be at the expected pile tip elevation for an end-bearing pile.

(b) A drawdown of groundwater table would also induce NSF on the pile. However, owing to temporary increase in the soil effective stress due to rapid water drawdown in the top sand layer while the dissipation of pore pressure in the clay has not really started, there is a temporary ground heave and reduction of NSF during the initial drawdown period. After the excess pore pressure in the clay started to dissipate, NSF started to develop again along the pile.

(c) For pile installation and water drawdown, it is noted that NSF has not been fully mobilized at and close to the pile tip location, as expected, due to negligible relative pile-soil settlement around NP. When conventional total stress α or effective stress β method is used, both methods would overestimate the magnitude of NSF induced on the pile as both methods assume full mobilization of NSF from ground surface till the neutral point.

(d) The application of load on the pile would reduce the magnitude on the pile due to transfer of applied load along the pile shaft. On the other hand, the application of different magnitudes of surcharge inducing various magnitudes of ground settlement would result in different degrees of mobilization of NSF at and close to the pile tip. The larger the induced soil settlement around the pile shaft due to larger surcharge intensity, the larger is the degree of mobilization of NSF on the pile.

(e) For the present relatively short end-bearing piles, it is established that a large percentage of transient live loads is transferred to the NP contributing to the maximum axial force in the pile, in contrary with existing postulation that transient live loads need not be considered for a pile subject to NSF.

To further understand the mechanism of end-bearing pile subject to NSF, numerical FEM analyses were conducted. The following findings are noted:

(a) If the correct friction angle of the soil-pile interface element is adopted, the NSF induced on an end bearing pile measured from the above centrifuge model study can be correctly simulated using either the Mohr Coulomb or the Modified Cam Clay model.

(b) Under the same pile slenderness ratio L/d, the degree of mobilization increases with surcharge intensity, but tends to taper off after the surcharge intensity is beyond 40 kPa. On the other hand, increase in pile-soil stiffness ratio K tends to increase the degree of mobilization of

NSF, but with a smaller influence for stocky pile with L/d of 12 and a larger influence on slender pile with L/d of 48.

(c) Although there are some field data which suggests that transient live loads dissipates along the pile shaft and never reaches the NP and thus need not be considered when evaluating the maximum NSF at NP, the present study demonstrates that the percentage of transient live loads transferred to NP increases with increasing pile-soil stiffness ratio and decreasing pile slenderness ratio. Only with very large pile slenderness ratio of ratio of over 90, and very low pile-soil stiffness ratio of less than 1000, can the percentage of transient live loads transferred to the neutral point be reasonably neglected.

(d) Charts are provided in this paper to facilitate an estimation of degree of mobilization of NSF and percentage of live loads that would be transferred to the NP contributing to the maximum load on end-bearing piles under various pile and soil conditions.

Acknowledgments

The writers wish to acknowledge the help rendered by the laboratory technologists in the Geotechnical Centrifuge Laboratory of the National University of Singapore for their able and kind assistance in conducting the centrifuge tests for the present study.

References

Auvinet, G. and Hanell, J.J. (1981), "Negative skin friction on piles in Mexico city clay", *Proceedings of 10th International Conference of Soil Mechanics and Foundation Engineering*, **2**, 599-604.

Bozozuk, M. (1981), "Bearing capacity of pile preloaded by downdrag", *Proceedings of 10th International Conference of Soil Mechanics and Foundation Engineering*, **2**, 631-636, June.

Burland, J.B. (1973), "Shaft friction of piles in clay", *Ground Eng*., **6**(3), 30-42.

Davisson, M.T. (1993), "Negative skin friction in piles and design decision", *Proceeding of 3rd International Conferences of Case Histories Geotechnical Engineering*, St. Louis, Missouri, 1792-1801, June.

Fellenius, B.H., (1972), "Downdrag on piles in clay due to negative skin friction", *Can. Geotech. J*., **9**(4), 323-327.

Fellenius, B.H., (2006), "Results from long-term measurement in piles of drag load and downdrag", *Can. Geotech. J*., **43**(4), 409-430.

Gao, H.M. Liu, H.L., Liu, J.Y. and Liu, M.L. (2011), "Back calculated alpha and beta coefficients from case histories of negative skin friction piles", *Mater. Res. Innov*., **15**(1), 597-600.

Garlanger, J.E. (1974), "Measurement of pile downdrag beneath a bridge abutment", *Highway Research Board*, *Transport Research Record*, **517**, 61-69.

Indraratna, B., Balasubramaniam, A.S., Phamvan, P. and Wong, Y.K. (1992), "Development of negative skin friction on driven piles in soft Bangkok clay", *Can. Geotech. J*., **29**(3), 393-404.

Inoue, Y., Tamaoki, K. and Ogai, T. (1977), "Settlement of building due to pile downdrag", *Proceedings of 9th International Conference of Soil Mechanics and Foundation Engineering*, Tokyo, Japan, **1**, 561-564, May.

Jacob, F. and Kenneth, L.C. (1997), *Construction Failure*, (2nd Edition), John Wiley and Sons, Inc., New York.

Johannessen, I.J. and Bjerrum, L., (1965), "Measurement of the Compression of a Steel Pile to Rock due to Settlement of the Surrounding Clay", *Proceedings of 6th International Conference of Soil Mechanics and*

Foundation Engineering, Montreal, Canada, **2**, 261-264, August.
Kog, Y.C. (1987), "A case study of downdrag and axial load on timber piles in layered soil", *Proceedings of 5th International Geotechnical Seminar on Case Histories in Soft Clay*, Nanyang Technological Institute, Singapore, 269-276, December.
Kog, Y.C. (1990), "Down-drag and axial load on piles", *Ground Eng*., 24-30.
Lam, S.Y., Ng, C.W.W., Leung, C.F. and Chan, S.H. (2009), "Centrifuge and numerical modeling of axial load effects on piles in consolidating ground", *Can*. *Geotech*. *J*., **46**(1), 10-24.
Lee, C.J., Chen, H.T. and Wang, W.H. (1998), "Negative skin friction on a pile due to excessive groundwater withdrawal", *Proceeding of Centrifuge 98*, 513- 518, Rotterdam, September.
Lee, C.J., Bolton, M.D. and Al-tabbaa, A. (2002), "Numerical modeling of group effects on the distribution of dragloads in pile foundations", *Geotech*., 52(5), 325-335.
Lee, C.J., Lee, J.H. and Jeong, S. (2006), "The influence of soil slip on negative skin friction in pile groups connected to a cap", *Geotech*., **56**(1), 53-56.
Leung, C.F., Liao, B.K., Chow, Y.K., Shen, R.F. and Kog, Y.C. (2004), "Behavior of pile subject to negative skin friction and axial load", *Soil*. *Found*., **44**(6), 17-26.
Leung, C.F., Radhakrishnan, R. and Tan, S.A. (1991), "Performance of precast driven piles in marine clay", *J*. *Geotech*. *Eng*., *ASCE*, **117**(4), 637-657.
Matyas, E.L. and Santamarina, J.C. (1994), "Negative skin friction and the neutral plane", *Can*. *Geotech*. *J*., **31**(4), 591-597.
Ng, C.W.W., Poulos, H.G. and Chan V.S.H. (2008), "Effects of tip location and shielding on piles in consolidating ground", *J*. *Geotech*. *Geoenviron*. *Eng*., **134**(9), 1245-1260.
Poulos, H.G. and Davis, E.H. (1980), *Pile foundation analysis and design*, John Wiley and Sons, Inc., New York.
Singapore Standard CP4 (2003), *Code of Practice for Foundations*, published by Standardization Department, SPRING Singapore, ISBN 9971-67-914-0.
Tomlinson, M.J. (1994), *Pile Design and Construction Practice*, (4th Edition), Taylors and Francis.
Wood, D.M. (1990), *Soil Behaviour and Critical State Soil Mechanics*, Cambridge University Press, Cambridge, England.

CC